Proceedings of the 21st ICSMGE, Vienna, Austria, 14 – 19 June 2026. Pistrol, Adam & Schweiger (eds.)
Published by: ÖGG, Austrian Society for Geomechanics, Salzburg, Austria, ISBN 978-3-9503898-4-5
https://doi.org/10.53243/ICSMGE2026-1821

Laboratory investigation of primary wave velocities and constrained moduli of glauconite sand under anisotropic stress states

Shuyin Feng
Department of Architecture and Built Environment, Birmingham City University, United Kingdom, shuyin.feng@bcu.ac.uk

Parham Reyhanianasl, Mingnan Li, Chris Brandish-Lowe, Toby Masters
Geoquip Marine, United Kingdom

Erdin Ibraim, Tingfa Liu, Andrea Diambra
School of Civil, Aerospace and Design Engineering, University of Bristol, United Kingdom

ABSTRACT: Glauconitic materials pose significant challenges for the installation and design of offshore pile foundations. Evaluation of the primary wave velocities (V_P) of geo-materials is an essential step for their geophysical and dynamic characterisation. The extender element test method measures the V_P of geo-materials by applying a high-frequency pulse excitation, typically between 5 and 50 kHz. Recent advancement in the extender element test proves its effectiveness for utilization in both laboratory research and industrial applications. In this study, an advanced dynamic triaxial apparatus equipped with a pair of combined bender/extender element inserts was used to measure the V_P of glauconitic sand. The glauconite samples were subjected to the designed deviatoric stress paths to investigate the effects of anisotropic stress states on V_P. All samples were prepared and tested in dry states to avoid the mask signal effects from pore water. Detailed information of the specimen density and straining under the applied isotropic and anisotropic stress paths was acquired by high-resolution local strain sensors. The effects of stress anisotropy were highlighted by normalising the measured small strain constrained moduli (M_{max}) with respect to a void ratio function and their corresponding values at isotropic stress states. The crushing potential of glauconitic sand has also been assessed. The results indicate that at a given effective mean stress p', the normalised M_{max} of the tested samples increased with the applied stress ratio (q/p'), while no significant crushing has been observed in the samples tested under mean effective stress level up to 600 kPa.

KEYWORDS: Glauconitic sand, primary wave velocity, small strain constrained modulus, stress ratio, bender/extender elements, crushing potential

1 INTRODUCTION

Glauconitic sand is widespread and a peculiar geotechnical material, especially in offshore engineering settings, due to its high susceptibility to particle breakage (e.g., Westgate et al., 2023a, b, DeGroot et al., 2023, Konstantinou et al., 2025). The crushing potential of glauconite sand during cyclic action or stress change can pose challenges to foundation design and installation (Quinteros et al., 2023, Perikleous et al, 2023, Martinelli, et al., 2025) as well as in-situ testing such as cone penetration test (CPT) (Westgate et al., 2023b). Understanding the characteristics and behaviour of glauconitic material, while developing appropriate testing techniques, is crucial for the offshore engineering industry.

Stiffness of soils at small strain is crucial for evaluating deformation of geo-structures subjected to various stress states (He, 2018). To evaluate soil behaviour at very small strains, techniques such as resonant column testing and piezoelectric methods have been extensively utilized (Ishihara 1996). The bender element test, a type of piezoelectric method, has gained widespread adoption over the years for determining shear wave velocity (V_S) (Viggiani and Atkinson 1995; Jovicic et al. 1996). More recent developments have introduced the extender element test for the measurement of primary wave velocity (V_P), which has become increasingly popular in laboratory research (Lings and Greening, 2001; Leong et al. 2009; Kumar and Madhusudhan 2010).

Previous work on the small-strain stiffness has primarily focused on isotropic stress condition, even though soil is invariably subjected to anisotropic stress conditions. Payan et al. (2016) investigated the role of stress anisotropy on the shear modulus (G_{max}) of quartz sands and indicated that G_{max} of sands under anisotropic loading conditions are greater in magnitude than those subjected to isotropic stress states at a given mean effective stress p'. Senetakis et al. (2017) reported the constrained modulus M_{max} of quartz sands with different particle morphology under anisotropic stress conditions. This paper aims to investigate the M_{max} of glauconite sand under anisotropic stress state. Potential particle breakage of glauconite sand particles under varying stress paths is also examined.

2 EXPERIMENTAL METHODOLOGY

2.1 *Materials*

The glauconitic sand used in this study was sampled in the city of Antwerp, Belgium. Bulk X-ray diffraction (XRD) analysis indicates the collected material is composed primarily of glauconite (49.6% by weight) and quartz (39.3% by weight). Microscopic images of glauconitic sand grains are presented in Figure 1. The examined glauconite sand grains exhibit a predominantly rounded shape.

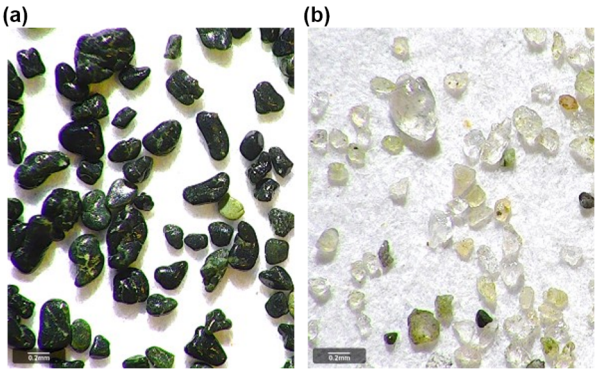

Figure 1. Microscopic image of the sediment after magnetic separation: (a) The magnetic fraction predominantly composed of glauconite grains; (b) The non-magnetic fraction; some pelletal glauconite traces remain

Figure 2 presents the particle size distribution of the air-dried sample, obtained following the sieving method as described in BS EN ISO 17892-4:2016 (BSI, 2016). The geotechnical index properties of the tested material and the corresponding methods are summarised in Table 1.

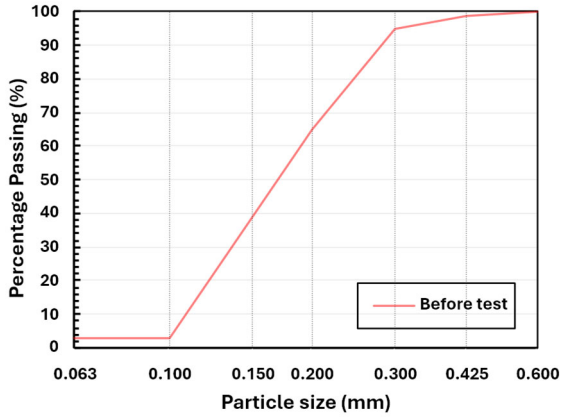

Figure 2. Particle size distribution of the sampled glauconite sand

Table 1. Index properties of the tested glauconite sand

Property	Value	Testing Method
G_S	2.68	BS EN ISO 17892-3:2015 pycnometer method by fluid displacement (BSI, 2015)
ρ_{min}	1.39 g/cm^3	NGI (2019a)
ρ_{max}	1.54 g/cm^3	NGI (2019b)
D_{50}	0.169 mm	BS EN ISO 17892-4:2016 (BSI, 2016)
C_U	1.76	
C_C	0.89	

2.2 *Test apparatus*

A GDS advanced dynamic triaxial testing system (DYNTTS), was employed for this study, as shown in Figure 3. The apparatus enables application of cell pressure up to 2 MPa.

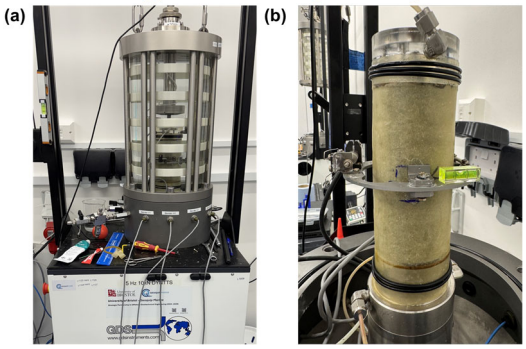

Figure 3. Apparatus and sample setup before tests

The apparatus houses piezo-element inserts functioning as both bender elements (BE) and extender elements (EE) (He and Senetakis, 2016; Senetakis et al., 2017; Li, 2018). The primary waves (P-waves) are generated and measured in EE mode, allowing the determination of primary wave velocity (V_P) and small-strain constrained modulus (M_{max}). The P-wave source is located at the base of the specimen, with the receiver fixed on the top cap. Axial strain during isotropic consolidation and the application of deviatoric stress is measured using a vertically mounted linear variable differential transformer (LVDT). A local radial strain gauge is attached at the specimen middle height (see Figure 3) to measure radial strains under both isotropic and anisotropic stress conditions.

2.3 *Experiment setup*

2.3.1 *Sample preparation*

Samples were prepared in a split mould with an internal diameter of 70 mm. The glauconite sand was air dried for at least 72 hours to avoid the potential changes in grain size caused by oven drying (King et al. 2023), before being lightly dry compacted into five layers in the mould. A 3D printed light Polylactic Acid (PLA) compactor of 41g self-weight was used to avoid potential disturbance from the sample preparation on the mechanical characteristics of glauconite sand (Westgate et al. 2023b). The samples were compacted to a final height of 140 mm with a relative density (D_r) ≈55%.

2.3.2. *Testing programme*

The prepared samples were isotopically consolidated at the designated initial effective confining pressures σ'_3 at 200 kPa (Sample 1), 400 kPa (Sample 2), and 600 kPa (Sample 3). All samples were consolidated and tested in a dry state to ensure reliable P-wave velocities measurements by eliminating the mask signal effect from saturation (Leong and Cheng, 2016), hence the effective stress σ' is equal to the total stress σ at all testing stages. Following consolidation, a deviatoric compressive stress (q) was applied while maintaining a constant mean effective stress p' (i.e., increasing the effective axial stress σ'_1 while decreasing the effective confining effective stress σ'_3). P-wave velocities (V_p)were measured from extender element tests with a pulse excitation of sinusoidal input at the following applied stress ratios: q/p' = 0, 0.25, 0.5, 0.75, 1, 1.25. A reference input frequency 25 kHz was used for further interpretation based on the quality of the signals. Volumetric strains throughout the test were acquired by the LVDTs and the local strain gauge. The M_{max} was obtained using the calculated density (ρ) from the measured volumetric strains, following Equation (1):

$$M_{max} = \rho \times V_p^2 \quad (1)$$

To examine the effect of stress history on the stiffness of glauconite sand, constant mean effective stress p' at 400 kPa and 600 kPa were then applied to the sample 1 (consolidated at an initial effective confining pressure of 200 kPa), with the P-wave velocities (V_p) being measured at the designated applied stress ratio q/p' before unloading. Figure 4 presents the complete designated stress path followed for Sample 1.

Table 2 summarises the initial unit weight (γ_0), void ratio (e_0), sample weight (m_0), height (H_0) and diameter (d_0) under vacuum supporting before testing, and the mean effective stress p' at which the extender element tests were performed for all three samples.

Particle size distribution tests were carried out to examine potential particle breakage upon the completion of dynamic test for each sample, following BS EN ISO 17892-4:2016 (BSI, 2016).

Table 2. Sample initial characteristics and dynamic testing programme ("S1" - Sample 1; "S2" – Sample 2; "S3" – Sample 3)

Sample	γ_0 (kN/m^3)	e_0	m_0 (g)	H_0 (mm)	d_0 (mm)	P' reached (kPa)
S1	14.41	0.82	801.3	140.55	70.29	200, 400, 600
S2	14.22	0.85	801.3	140.96	70.67	400
S3	14.53	0.81	801.3	139.70	70.23	600

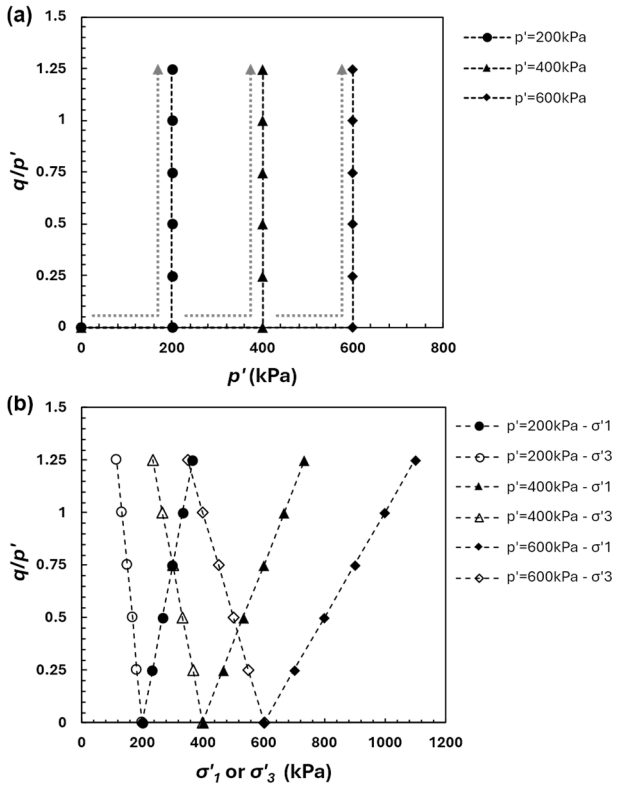

Figure 4. Designated stress paths applied in the extender element tests for Sample 1: (a) q/p' against p'; (b) q/p' against σ'_1 and σ'_3

3 RESULT

3.1 *P - wave signal interpretation*

Typical signal interpretation of extender element tests for sample 1 at p' = 200, 400 and 600 kPa under isotropic stress states by the end of consolidation stage is presented in Figure 5. Both the first-time-arrival and peak-to-peak methods provide a clear identification of the received signals.

A comparison of the measured V_p based on both methods for Sample 1 at isotropic and anisotropic stress states is presented in Figure 6. The results show good agreement between the two approaches for P-wave signal interpretation. The peak-to-peak method was subsequently used for the measurement of V_p and M_{max} in this study.

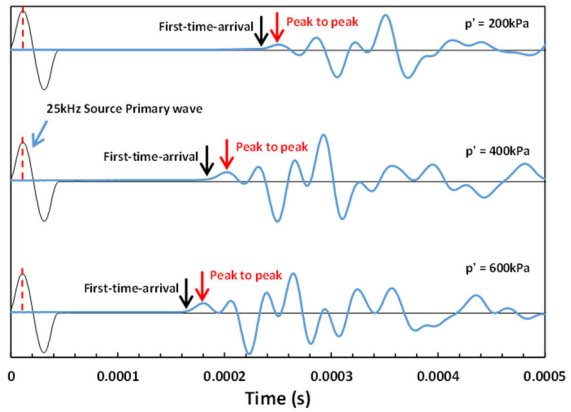

Figure 5. Signal interpretation of extender element tests under different p' condition (data collected from S1 at isotropic stress states)

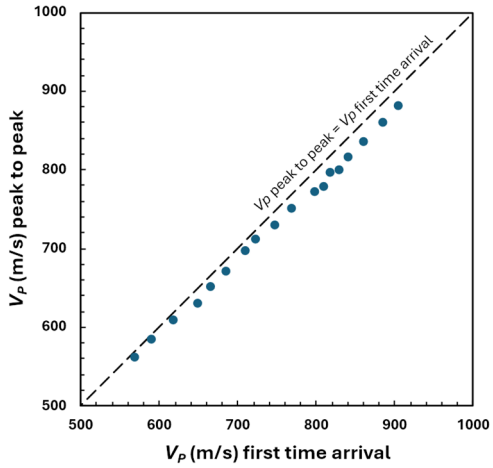

Figure 6. V_P determined based on peak-to-peak method versus first-time- arrival method (data collected from sample 1 at both isotropic and anisotropic stress states)

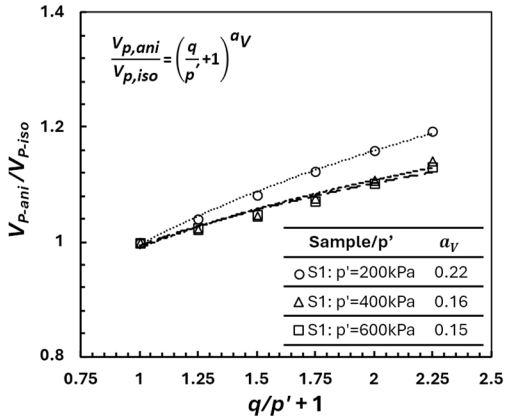

Figure 7. Effect of stress anisotropy on the normalised V_p for S1 at all applied p' level

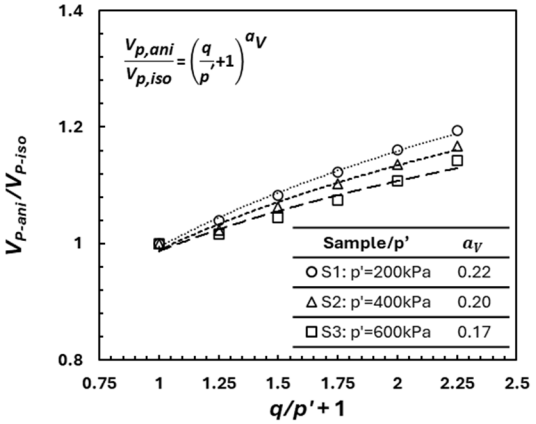

Figure 8. Effect of stress anisotropy on the normalised V_p for S1, S2 and S3 at the applied initial p' levels

Measured V_p at anisotropic stress states ($V_{p,ani}$) for all tested samples are normalised by the corresponding V_p measured under isotropic stress conditions ($V_{p,iso}$), and plotted against the stress ratio (q/p'+1), as shown in Figure 7 and Figure 8, following the formula given by Senetakis et al. (2017):

$$\frac{V_{p,ani}}{V_{p,iso}} = \left(\frac{q}{p'} + 1\right)^{a_V} \quad (2)$$

Where a_V is an exponent that describes the sensitivity of V_p to stress anisotropy. The results indicate that $V_{p,ani}$ increases with increasing stress ratio q/p' (i.e., with increasing q) for all tested samples. The influence of stress anisotropy on the normalised V_p is more pronounced at lower p' stress level. However, such trend is less evident under the stress path condition for Sample 1 at p' = 400kPa and p'= 600 kPa.

3.2 M_{max} at isotropic stress states

Constrained modulus M_{max} under both isotropic and anisotropic stress conditions for all tested samples was calculated using Equation (1), based on the measured V_p and specimen density (ρ) derived from volumetric strain measurements. The influence of the sample's e and the mean effective stress p' on the dynamic properties of soil has been extensively studied (e.g., Hardin and Black, 1968; Iwasaki et al., 1978; Saxena and Reddy, 1989; Menq, 2003; Wichtmann and Triantafyllidis, 2010). A void ratio function $f(e) = e^{-1.3}$ is adopted (after Jamiolkowski et al., 1991) in this study. A power-law form is used to correlate the normalised constrained modulus $M_{max}/f(e)$ with the normalised mean effective pressure (by a unit pressure of 1 kPa in this study), as expressed in Equation (3):

$$\frac{M_{max}}{f(e)} = A \times \left(\frac{p'}{1}\right)^n \quad (3)$$

where A is a material constant and n is an exponent that indicates the sensitivity of the constrained modulus to pressure.

Figure 9 and Figure 10 show the normalised $M_{max}/f(e)$ against p' for Sample 1 at different p' stress level and for Samples 1 to 3 at the applied initial p' stress states, respectively, both indicating increasing $M_{max}/f(e)$ with increasing stress level. A slightly higher exponent n is observed in Figure 9, which may be attributed to the applied stress histories for Sample 1.

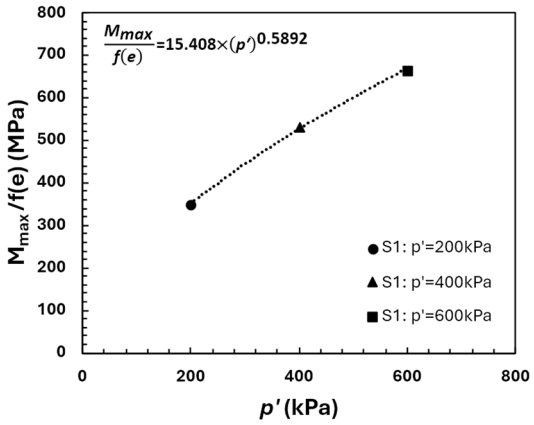

Figure 9. $M_{max}/f(e)$ versus p' for S1 at all applied p' level

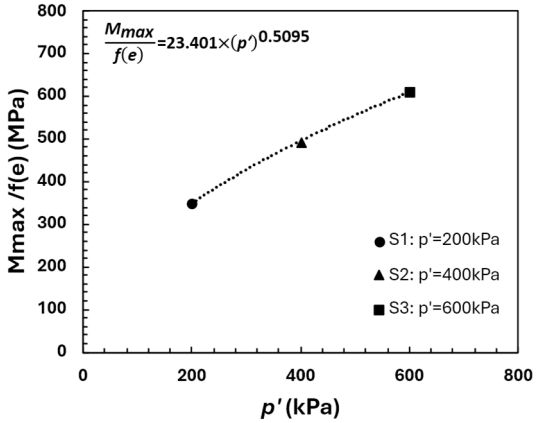

Figure 10. $M_{max}/f(e)$ versus p' for S1, S2, S3 at the applied initial p'

3.3 M_{max} at anisotropic stress states

To examine the effect of stress anisotropy on M_{max} for the tested glauconite sand samples, a general expression form proposed by Payan et al. (2016) is adopted:

$$M_{max,normalised} = \frac{M_{max,ani}/f(e_{ani})}{M_{max,iso}/f(e_{iso})} = \left(\frac{q}{p'} + 1\right)^{a_M} \quad (4)$$

where $M_{max,ani}$ and $f(e_{ani})$ are the constrained modulus and void ratio function at anisotropic stress states, $M_{max,iso}$ and $f(e_{iso})$ are the constrained modulus and void ratio function under isotropic confining pressures p', a_M is the regressed exponent to assess the effect of stress ratio (stress anisotropy) on the normalised M_{max}.

Figure 11 and Figure 12 present the $M_{max,normalised}$ against q/p'+1 for all the tested samples. It can be observed that normalised M_{max} increase invariably with increasing q/p'. In addition, the regressed a_M decrease at increasing p'. Similar trends were observed by Li (2018) on recycled concrete aggregate materials. The regressed a_M for Sample 1 at p' = 400 and 600kPa are lower than those found for Sample 2 and 3 along the same anisotropic stress paths, reflecting potential effects of the applied stress history.

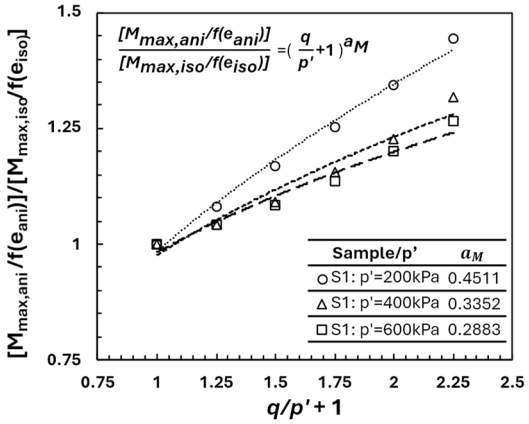

Figure 11. Normalised constrained modulus $M_{max,normalised}$ against q/p'+1 for S1 at all applied p' levels

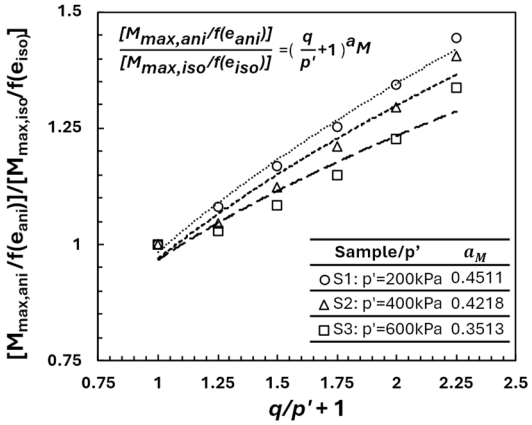

Figure 12. Normalised constrained modulus $M_{max,normalised}$ against q/p'+1 for S1, S2, S3 at the initial applied p' level

Figure 13 compares the normalised constrianed modulus $M_{max,normalised}$ for all tested glauconite sand samples at the initial applied mean effective stress p' levels with the results reported by Senetakis et al. (2017) on white sand, a quartz sand with similar grain sizes and shapes to the tested glauconite sand. The overall trend matches well. Under the same anisotropic stress paths, the regressed a_M values of the glauconite sand are consistently higher than those of the white sand, which may be

attributed to the differences in the governing minerals in these materials. Further experimental investigation and quantitative analysis is required to corroborate this finding.

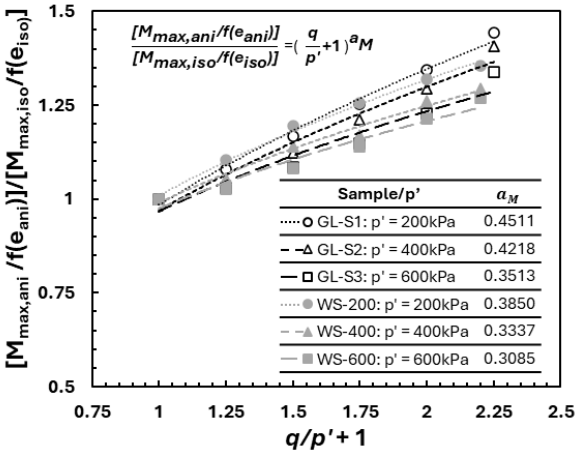

Figure 13. Comparison of test results for glauconite sand (GL) and white sand (WS, data from Senetakis et al. 2017)

3.4 *Particle size distribution variation*

Figure 14 presents the particle size distributions (PSD) of the glauconite sand materials after relative density tests, and before and after each dynamic tests, indicating no significant change. Note that all the PSD tests were conducted using the same sieve set. Some variations may be noticed comparing the post test PSD of S1 with those of S2 and S3, with S1 showing a slight higher percentage of particles smaller than 0.2 mm. This difference potentially indicates a minor degree of particle crushing induced by the unloading-reloading stress paths applied on S1 during the dynamic wave testing.

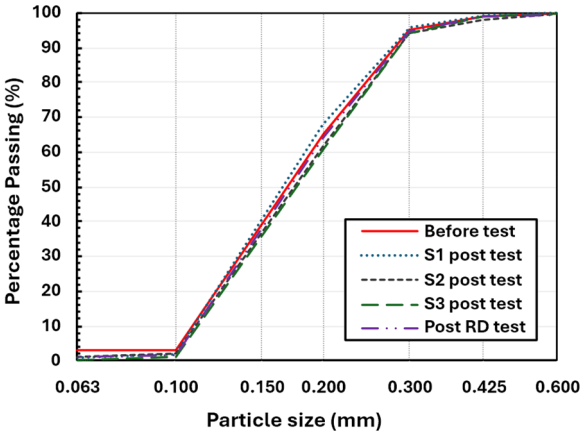

Figure 14. Particle size distribution before and after test: "post-test"- upon the completion of dynamic test; "post RD test" – upon the completion of relative density test

4 CONCLUSIONS

This study presents results on the P-wave velocity (V_p) and maximum constrained modulus (M_{max}) of natural glauconite sand from onshore Belgium. Testing was performed in an advanced dynamic triaxial apparatus equipped with combined bender/extender elements. Three samples were initially consolidated isotropically before being subjected to designated anisotropic stress paths with stress ratios *q/p'* up to 1.25 while maintaining constant *p'*. Sample 1 was subjected to unloaded and reloaded stress paths for further dynamic testing under various stress conditions. P-wave velocities were measured following the peak-to-peak method.

The results show that V_p and normalised M_{max} increased with increasing *q/p'* at a given *p'*, with greater sensitivity at lower *p'* levels. The tested Glauconite sand shows systematically higher sensitivity to stress anisotropy, as indicated by higher regressed a_M values, when compared to white sand of similar gradation and particle shape. The particle size distribution analysis shows no substantial post-test changes for the samples tested in this study, although a minor degree of particle crushing was observed in the sample subjected to repeated unloading–reloading stress path.

The experimental results indicate that, when modelling the small-strain dynamic behaviour of glauconitic sand, stress anisotropy, stress history and mineralogical composition (i.e., glauconite content) should be explicitly considered to account for their potential influence on dynamic modulus–stress relationships. This study focused on one single type of glauconitic sand under relatively limited density and stress conditions. Further studies on other glauconitic sands with varying gradation and particle shapes and under wider ranges of test conditions are required to further enhance and enrich the research findings.

5 ACKNOWLEDGEMENTS

This study was undertaken as part of a Strategic Partnership between Geoquip Marine and the University of Bristol. The authors thank the laboratory team of Geoquip Marine for their support on the research. The presented classification and dynamic wave tests were conducted at Geoquip Marine Bristol Laboratory. The authors would also like to thank Dr Rieko Adriaens of Qmineral for conducting the minerology analysis.

6 REFERENCES

British Standards Institution (BSI). 2015. *ISO 17892-3:2015 Geotechnical investigation and testing. Laboratory testing of soil - Determination of particle density*. London: BSI.

BSI. 2016. *BS EN ISO 17892-4:2016 Geotechnical investigation and testing. Laboratory testing of soil - Determination of particle size distribution*. London: BSI.

DeGroot, D. J., Westgate, Z. J., and Yetginer-Tjelta, T. I. 2023. Geological and geotechnical challenges of the East Coast United States for offshore energy transition. *Proceedings of 9th International SUT Offshore Site Investigation and Geotechnics Conference: Innovative Geotechnologies for Energy Transition*, 82–111.

Geyin, M., Madyorava, M. M., Dantal, V., Kassa, H. M. 2023. An SBI-based interbeddedness index for the prediction of glauconitic material for offshore geotechnics. *Proc. 9th International SUT Offshore Site Investigation and Geotechnics Conference: Innovative Geotechnologies for Energy Transition*, London, 112-117.

Hardin, B. O. and Black, W. L. 1968. Vibration modulus of normally consolidated clay. *Journal of Soil Mechanics & Foundations Division*, ASCE 94(2), 353-369.

He, H., 2018. *Dynamic properties of crushable soils*. Doctoral dissertation, UNSW Sydney.

He, H., and Senetakis, K. 2016. A study of wave velocities and Poisson ratio of recycled concrete aggregate. *Soils and Foundations*. 54(6), 593–607.

Ishihara, K. 1996. *Soil behaviour in earthquake geotechnics*. Oxford Science Publications, Oxford.

Iwasaki, T., Tatsuoka, F. and Takagi, Y. 1978. Shear moduli of sands under cyclic torsional shear loading. *Soils and Foundations* 18(1), 39-56.

Jamiolkowski, M., Leroueil, S. & Lo Presti, D. (1991) Design parameters from theory to practice. In: Proceedings of the international conference on geotechnical engineering for coastal development. In Proceedings of Geo-Coast 1991, Coastal

Development Institute of Technology, Yokohama, Japan, pp. 877-917.

Jovicic, V., Coop, M. R., and Simic, M. 1996. Objective criteria for determining G_{max} from bender element tests. *Geotechnique*, 46(2), 357–362.

King, T., Wuenscher, T., Griffiths, L., and Fraps, A. 2023. A novel approach to quantifying glauconite content in soils using digital image analysis. *Proceedings of 9th International SUT Offshore Site Investigation and Geotechnics Conference: Innovative Geotechnologies for Energy Transition*, 118-123.

Konstantinou, M., Piedrabuena, A. R., Hellebrekers, N., Elkadi, A. S., Mento, M., and Gavin, K. 2025. Geotechnical Properties of a Glauconite Sand from Belgium. Proc. *ISFOG 2025, Nante.*

Kumar, J., and Madhusudhan B. N. 2010. Effect of relative density and confining pressure on Poisson ratio from bender and extender elements tests. *Geotechnique* 60(7),561–567.

Leong, E. C., and Cheng, Z. Y. 2016. Effects of Confining Pressure and Degree of Saturation on Wave Velocities of Soils. *International Journal of Geomechanics*, 16(6).

Leong, E. C., Cahyadi, J., and Rahardjo, H. 2009. Measuring shear and compression wave velocities of soils using bender-extender elements. *Canadian Geotechnical Journal*, 46, 792–812.

Li, M. 2018. *Study of mechanics and dynamics of fibre reinforced recycled concrete aggregate*, UNSW Sydney.

Lings, M.L. and Greening, P.D., 2001. A novel bender/extender element for soil testing. Géotechnique, 51(8), pp.713-717.

Martinelli, M., Konstantinou, M., Tamagnini, C., Gavin, K., Thijssen, R., and van Giffen, I. 2025. SICMOG: Site Characterization and Monopile Installation in Glauconite Soils. In C. Abadie, L. Thorel, M. Blanc, & Z. Li (Eds.), *Proc. ISFOG 2025, Nante.*

Menq, F.-Y. 2003. *Dynamic properties of sandy and gravelly soils*, Doctor of Philosophy, University of Texas at Austin, USA.

NGI. 2019a. *Recommended method statement – Determination of minimum dry density of sands*.

NGI. 2019b. *Recommended method statement – Determination of maximum dry density of sands*.

Payan, M., Khoshghalb, A., Senetakis, K. and Khalili, N., 2016. Small-strain stiffness of sand subjected to stress anisotropy. *Soil Dynamics and Earthquake Engineering*, *88*, 143-151.

Perikleous, G., Meissl, S., Diaz, A. T., Stergiou, T., and Ridgway-Hill, A. 2023. Monopile installation in glauconitic sand. *Proc. 9th International SUT Offshore Site Investigation and Geotechnics Conference: Innovative Geotechnologies for Energy Transition*, London, 132–138.

Quinteros, V. S., Westgate, Z., Vinck, K., Dantal, V., Lindtorp, A., Toma, M. A. 2023. Interface friction angle of galuconitic sands for pile design. *Proc. 9th International SUT Offshore Site Investigation and Geotechnics Conference: Innovative Geotechnologies for Energy Transition*, London, 155-161.

Saxena, S. K. and Reddy, K. R. 1989. Dynamic moduli and damping ratios for Monterey no. 0 sand by resonant column tests. *Soils and Foundations* 29(2), 37-51.

Senetakis, K., Li, M., He, H. and Ranjith, P.G., 2017. Experimental investigation of primary-wave velocities and constrained moduli of quartz sand subjected to extender element tests and stress anisotropy. *Geomechanics and Geophysics for Geo-Energy and Geo-Resources*, *3*(2), 211-219.

Viggiani, G., and Atkinson, J. H. 1995. Interpretation of bender element tests. *Geotechnique,* 45(1),149–154.

Westgate, Z. J., Beemer, R. D., DeGroot, D. J. 2023a. Implications of glauconite sand on US offshore wind development. *Proc. 9th International SUT Offshore Site Investigation and Geotechnics Conference: Innovative Geotechnologies for Energy Transition*, London, 124–131.

Westgate, Z. J., DeGroot, D. J., McMullin, C., Zou, Y., Guo, D., van Haren, S., Beemer, R. D., Zeppilli, D., Miller, K. G., and Browning, J. 2023b. Effect of degradation on geotechnical behavior of glauconite sands from the U.S. Mid-Atlantic Coastal Plain. *Ocean Engineering*, 283, 115081.

Wichtmann, T., and Triantafyllidis, T. 2010. On the influence of the grain size distribution curve on P-wave velocity, constrained elastic modulus M_{max} and Poisson's ratio of quartz sands. *Soil Dynamics and Earthquake Engineering*, *30*(8), 757-766.